POAC'13
Espoo, Finland

Proceedings of the 22nd International Conference on
Port and Ocean Engineering under Arctic Conditions
June 9-13, 2013
Espoo, Finland

MEASUREMENTS OF PACK ICE STRESSES IN THE BALTIC

Mikko Lensu[1], Mikko Suominen[2], Jari Haapala[1], Reino Külaots[2], Bruce Elder[3]
[1]Finnish Meteorological Institute, Helsinki, Finland
[2]Aalto University, Espoo, Finland
[3] USACE Engineer Research and Development Center, Cold Regions Research and Engineering Laboratory, Hanover, New Hampshire, USA

ABSTRACT
Wind and oceanic forcing generates dynamic stresses in a compact ice cover. To this is related the stress propagation phenomenon where stress is transmitted along chains of contacting floes. To the ice navigation community ice stresses manifest as compression that closes channels and slows down ship's progress. The including of compression to ice forecasts is the aim of SAFEWIN project. This development work and the relating of the model quantities to the forces a ship actually experiences requires understanding of how ice cover stresses are generated and transmitted. Experimentally this can be approached in terms of local ice stress measurements that are then compared with the larger scale values from the ice forecast model. Results of a two-week stress campaign conducted in the Bay of Bothnia in 2011 are described. The measurement site was on a floe that drifted to NE direction close to Tankar lighthouse and the 1 hour average wind speed was mostly above 10 m/s. The instruments included a biaxial stressmeter of the same type as has been used in Arctic campaigns, and two arrays of pressure cells. The principal stresses were calculated by rosette theory and the difference between major and minor principal stress was interpreted as dynamic stress magnitude. The dynamics stress had intermittent character with peaks separated by low stress periods and the maximum stresses were about 80 kPa. The peaks could be related to several types of events: dynamic drift, ridging, stress buildup in static ice cover, and stress buildup when ice converges against coast. The results from the biaxial stressmeter and the arrays had a good correlation for the occurrence of stress peaks while stress values could be different.

INTRODUCTION
For low concentrations the ice cover drifts as a collection of individual floes. The momentum balance equation describing the drift includes terms for the momentum fluxes between the floes, atmosphere and the ocean. As concentration increases and the floes start getting into contact this introduces contact stresses and a momentum flux between the floes. In a compact ice cover the atmospheric and oceanic forcing generates a complicated stress state that slows down the drift, and drives ridging and compression. From an ice navigating ship's viewpoint compression manifests as local strains and ice pressure. Channels are closed and ship speed is reduced or the progress is stopped altogether. Pileup and hull damage can occur in difficult compressive conditions.

The objective of SAFEWIN project is to include ice compression in ice forecasts (Lensu and others, 2013a) and to connect the modelled compression with the local stresses affecting ships. Understanding of the spatial and temporal variation of stresses requires measurements. This can be realised by instrumenting floes by stressmeter arrays. Several stress measurement

campaigns have been conducted in the Arctic during the last 25 years. Earlier campaigns used pressure cell arrays (Croasdale and others, 1988, Coon and others, 1989) while later Arctic campaigns (Tucker and Perovich, 1992, Richter-Menge and Elder, 1998, Richter-Menge, Elder and others, 2002, Richter-Menge, McNutt and others, 2002) mostly used similar biaxial stressmeter as is described in Cox and Johnson (1983). All results exhibit intermittent, spiky stress records with maximum stresses of the order of 100-200 kPa.

Although some understanding on the stress magnitudes and stress record characteristics has been attained, the basic mechanisms generating stress concentrations to the ice cover are still not well known. Here the results from a two-week stress measurement campaign in the Baltic are described. Apart from the development of Baltic compression-resolving ice models they are expected to be relevant for the stress problem in general. The campaign was also interesting as a comparison of the two instrument types, pressure cells and biaxial stressmeters.

INSTRUMENTS AND METHODS

Biaxial stressmeter

The vibrating wire biaxial stressmeter is the main instrument in a stress buoy assembled by CRREL (US Army Corp of Engineers Cold Regions Research Engineering Laboratory). The buoy was deployed during the campaign by Finnish Meteorological Institute. The buoy determines also location and compass direction, and measures ice temperature of the stress gauge as well as air temperature. The data can be sent via satellite link.

The biaxial stressmeter was designed by CRREL in the beginning of 80's and is presently manufactured by Geokon Ltd. A calibration study on their use for ice stress measurements was made by Cox and Johnson (1983) and they were first successfully used to measure near field stresses in ice-structure studies. The biaxial stressmeter soon became a standard in Arctic campaign in 90's which improved the comparability of the results.

Biaxial stressmeter can be easily installed to any depth and needs little maintenance. It consists of a stiff steel cylinder, 0.25 m long and 57 mm wide and with 16 mm wall thickness. As the gauge modulus is about 200 GPa the measurements are not affected by variation in ice modulus. Inside the cylinder there are six wires tensioned at 30 degree intervals; three of these are sufficient for measurement, the remaining are for redundancy. The principal stress components are obtained from radial deformations of the cylinder, in turn determined from the resonant frequency of each wire. Cox and Johnson (1983) estimated 15% accuracy and 20kPa resolution for the gauges. Later the resolution was improved to 5 kPa.

Pressure cells

For the pressure measurements, Aalto University manufactured hydraulic pressure cells, or hollow metal plates about 10 cm in diameter and filled with ethanol. Pressure acting on the plate area distributes equally in the ethanol inside and is determined by a pressuremeter at the end of the pipe, Figure 1. Totally nine pressure cells of this type were manufactured. Five of these were attached to pressuremeters recording only the maximum pressure until next reset. Four pressuremeters sampled the pressure time history with the frequency of 20 Hz. The time histories were recorded by a data logger connected with cables to the pressuremeters. The logger and batteries were placed inside a weather resistant cover box.

Pressure cells are versatile, have simple operating principle and clear directionality, and can be manufactured to fit different expected stress ranges. They can either be frozen into the ice or forced to tight contact mechanically. Cell arrays can be designed flexibly to suit the conditions of the site and multiaxial measurements are possible with rosette arrays. Expendable arrays at potential ridge formation sites or close to structures can be realised with relatively low cost.

Calibration

The pressure cells were calibrated carefully before the expedition. The calibration was conducted with air pressure and with dead weights after freezing a device in ice. For calibration with air pressure, two concave metal parts were manufactured. These were attached together with bolts after the pressure plate was placed inside, see Figure 1. The air pressure was adjusted with a valve in the hose attached to calibration bench and measured with an analog pressuremeter. The results from the calibration of the pressure cells with air pressure are presented in Figure 2. It is seen the pressuremeter readings correspond the determined air pressure well for the expected range <200 kPa.

To define the effect of ice to the measurements with the pressure cells, calibration was conducted also with the pressure cells frozen in the ice block, see Figure 3. After the pressure cell had frozen in the ice, the recording of the pressure time history was started and dead weights were added on top of the ice block. The results from the calibration with dead weights are presented in Figure 3. The pressure determined with the dead weights is somewhat higher than the pressuremeter readings but the difference is small. The maximum pressure 50 kPa was not much lower than the highest values observed later in the field.

No calibration exercises were done for the biaxial stressmeters

Figure 1. Calibration with air pressure. The device on the left and device ready for air pressure calibration on right.

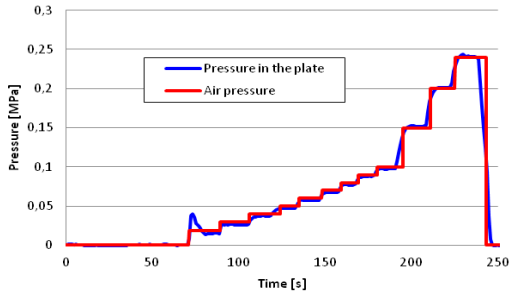

Figure 2. Calibration measurements with air pressure.

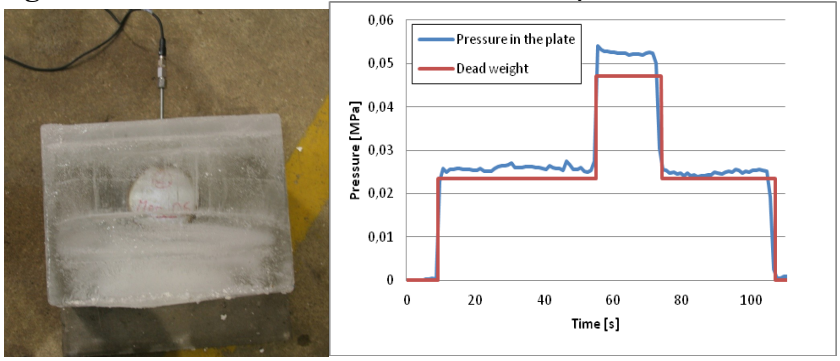

Figure 3. Device frozen in ice for calibration measurement (on the left) and measurements from the calibration tests (on the right).

Determination of principal stresses

Biaxial stressmeters are designed to resolve the two-dimensional stress state. The calculation of the principal stresses from the radial deformations of the steel cylinder, derived in turn from the resonant frequencies, is a lengthy but standard procedure described, for example, in Cox and Johnson (1983).

For the pressure cell array the principal stresses were calculated with rosette theory from a subarray of three cells arranged in 45 degree angles (Figure 4.)

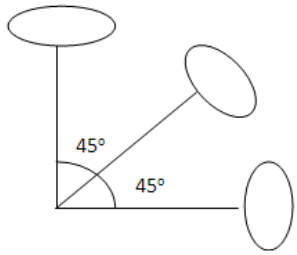

Figure 4. Schematic picture of the arrangement.

The strains in x- and y-direction and shear strain can be determined as follows

$$\varepsilon_x = \varepsilon_a$$
$$\varepsilon_y = \varepsilon_c \qquad (1)$$
$$\varepsilon_{xy} = \varepsilon_b - \frac{\varepsilon_a + \varepsilon_c}{2}$$

If the first two ones are multiplied with Young's modulus, E, and the last one with shear modulus, G, and Hooke's law $\sigma=\varepsilon E$ and $\tau=\gamma G=2\varepsilon_{xy}G$ is applied the following equations are obtained

$$\sigma_x = \sigma_a$$
$$\sigma_y = \sigma_c \qquad (2)$$
$$\tau_{xy} = \frac{2\sigma_b - \sigma_a - \sigma_c}{2(1+\nu)}$$

Now the principal stresses, $\sigma_{1,2}$, and the direction of the major stress, θ_p, can be calculated with the following equations

$$\sigma_{1,2} = \frac{\sigma_x + \sigma_y}{2} \pm \sqrt{\left(\frac{\sigma_x - \sigma_y}{2}\right)^2 + \tau_{xy}^2} \qquad (3)$$

$$\tan 2\theta_p = \frac{2\tau_{xy}}{\sigma_x - \sigma_y} \qquad (4)$$

Separation of dynamic and thermal stresses

The total stress state within the ice is summation of dynamic stress resulting from wind and currents, and thermal stress. The dynamic stress is assumed to affect wind direction and be aligned with the major principal stress. Thermal stress is assumed to be equal to all directions. According to the assumption, the major principal stress, σ_1, equals the dynamic stress plus the thermal stress, and the minor principal stress, σ_2, equals the thermal stress as the dynamic stress is affecting to the direction of major principal stress which is normal to the minor principal stress. Following from the assumptions, the dynamic stress can be calculated by reducing the minor principal stress form the major one. Although not completely unproblematic, this procedure has been standard in the Arctic campaigns (e.g. Richter-Menge and Elder, 1998) which establishes the comparability of dynamic stress estimates.

MEASUREMENTS

Instrument deployment and drift of the site

The stress measurement site was set up on 26 February 2011 during the first day of R/V Aranda cruise field camp. The location was in the southern Bay of Bothnia, about 40 km WSW from the Tankar lighthouse by the Kokkola channel. The pressure cells were collected on 4 March before when the camp was abandoned. The stress buoy was left on the site and was finally collected by helicopter on 28 April. However, the biaxial stressmeter lost soon its contact due to melting and the stress data after 10 March is not usable.

There were thus two measurement phases of 132 and 158 hours (Table 1). During the first phase all instruments were used, during the second phase only the biaxial stressmeter. Weather conditions were windy but remarkably persistent and the differences between the two phases were small. The average wind speed for the whole period was 9.1 m/s and for the two phases 9.4 m/s and 8.9 m/s respectively. Winds exceeding 10 m/s typically induced ice drift period. In addition to wind speed the wind direction changes had an important effect on the stress levels. The wind direction was otherwise in the SW quadrant but visited for two days the NW quadrant during the second phase.

The total net drift was 67 km to direction 51 and the drift direction remained within 15 degrees turning slowly clockwise. The ice cover was inert during the period of northerly winds. The drift speeds above creep velocities (>1.5 cm/s) were somewhat higher for the first period but as the fraction of inert periods was smaller during the second period the overall drift speed turned out to be about the same.

The campaign included in addition measurements on ice and snow thickness, surface roughness, snow and ice properties, aerial photography, and coastal radar and SAR images. Tankar coastal radar images are captured as a continuous activity by FMI for ice cover monitoring. After the field camp the stress buoy drifted through Tankar coastal radar image area which contained also drifter buoys and ice profiling sonar (Figure 5). During this period also an extensive helicopterborne EM thickness mapping was conducted in the area.

Table 1. Deployment, drift and weather data.

		Phase 1	Phase 2
Start time	hours	26 Feb 21:00	4 Mar 9:00
End time		4 Mar 9:00	10 Mar 23:00
Duration		132	158
Start location		63.79N 22.09E	63.97N 22.54E
End location		63.97N 22.54E	64.25N 22.94E
Net drift	km	31	36
Mean drift speed	cm/s	6.5	6.3
Maximum drift speed	cm/s	45.6	37.0
Net drift direction		43.6	57.3
Time fraction of drift > 1.5 cm/s	%	47	57
Mean drift speed > 1.5 cm/s	cm/s	14.0	11.0
Average temperature	°C	-1.5	-1.4
Minimum temperature	°C	-6.3	-8.5
Maximum temperature	°C	2.3	3.4
Average wind speed	m/s	9.4	8.9
Minimum 1 hour average wind	m/s	3.2	2.8
Maximum 1 hour average wind	m/s	16.1	13.4
Maximum wind gust	m/s	20.8	20.3
Average wind direction		222	240
Wind direction range		177-281	116-360

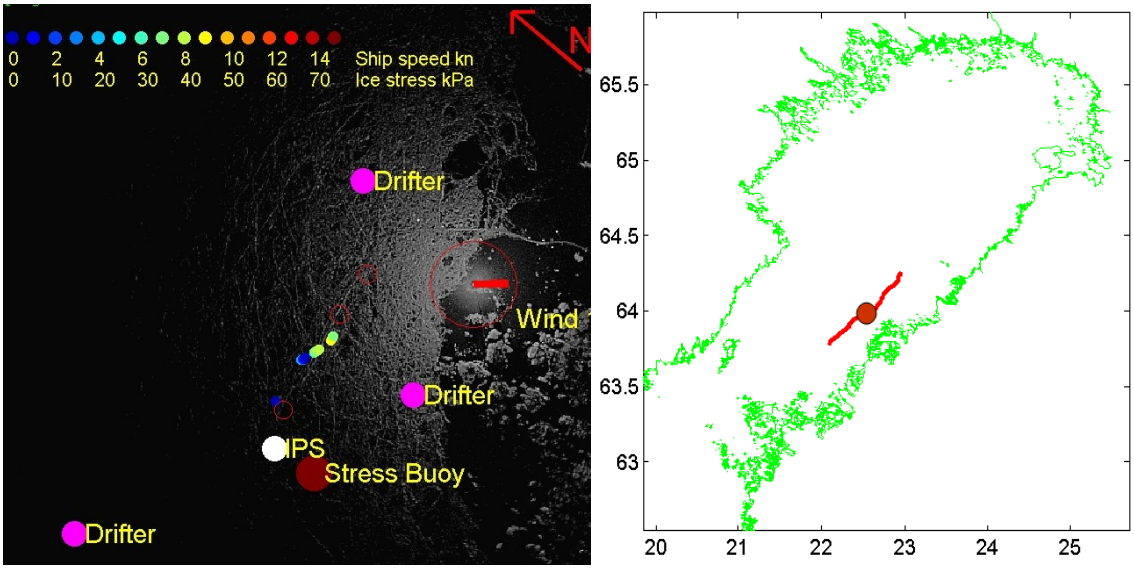

Figure 5. On the left the stress buoy on 6 March in the 40x40 km Tankar coastal radar image area. Other measurements in the area and AIS-retrieved ship speeds are also shown. On the right the same buoy location and buoy track during 26 February – 10 March 2011.

The site configuration and ice characteristics

The stress measurement site contained a pressure cell array, a cell array for maximum pressure, and the biaxial stressmeter of the stress buoy, Figure 6a. The pressure cells were installed into chainsaw slots at about 20 cm depth and let to freeze in contact. The pressure cell array had four pressure cells 2-3 m from the array center logger. Three of these formed a 45+45 degree rosette. The maximum pressure array had dimensions of about 100x50 meters and had five pressure cells with loggers displaying maximum pressure since the last reset. The data from the maximum array is not analysed here. The stress buoy was deployed about 30 from the pressuremeter logger with upper end about 10 cm from ice surface, Figure 6c.

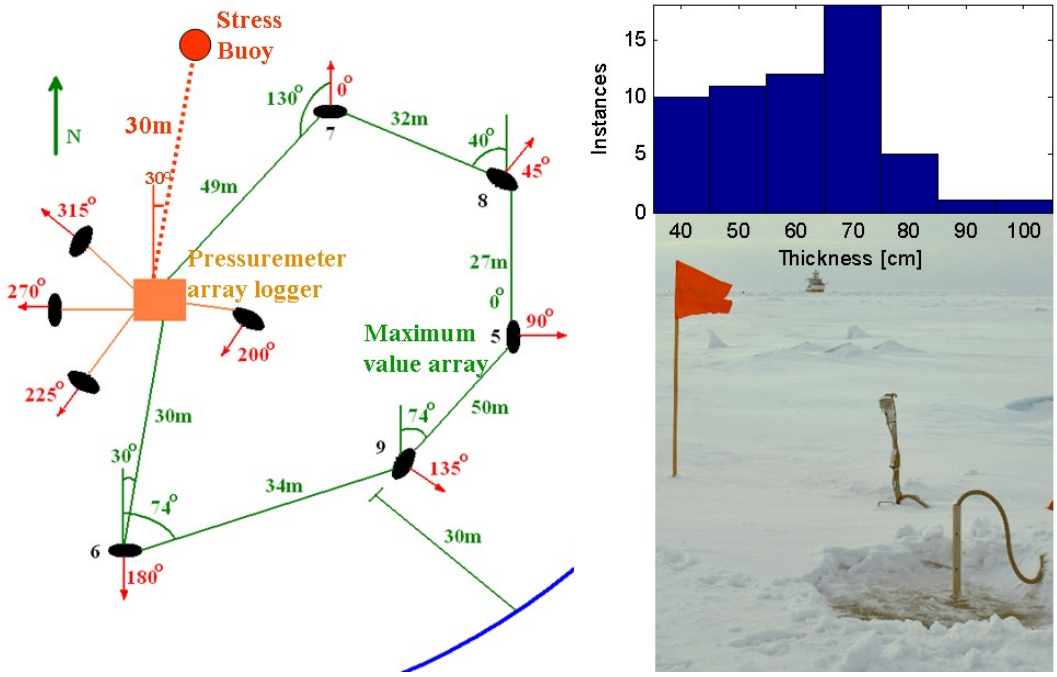

Figure 6. a) Schematic map of stress measurement site; closest crack with blue color, b)Ice thickness distribution at the site, and c) the stress buoy with the biaxial stressmeter (front) and temperature sensor visible.

The thickness of longer lines the made during the field camp varied between 40 and 60 cm, old rafted ice thickness was up to one meter and ridge keels less than 3 m. The ice type was rather slightly hummocked than ridged.

The measurement site was at a slightly larger level ice area than was typical for the surroundings but otherwise the ice type was similar. The level ice area was fringed by shallow ridges and the closest open crack was 30 m from the maximum array. Ice thickness around the biaxial stressmeter was measured from 12 locations within 4 m radius from the stressmeter. The mean thickness was 63 cm. The thickness around the pressure cell group was measured from 21 locations within 3 m radius and the mean thickness was 68 cm. Measurements were also done along the maximum pressure array and along line connecting the biaxial stressmeter and the pressure cell array. The overall mean thickness was 61 cm and the thickness histogram is in Figure 6b. The site can be characterised as level ice with some thickness variation that should not affect the results significantly.

RESULTS

Phase 1: Instrument comparison and local deformation

The Arctic stress campaigns have demonstrated that records from stressmeters close to each other can show, and typically do show, considerable differences. The stress spikes can occur at different times and have different magnitudes. On this background the correspondence between the dynamic stresses from the pressure cell array and from the biaxial stressmeter is surprisingly good, Figure 7. The days with full 24 hours of data are numbered from 1 to 5 for easier reference. Outside this range nothing important occurs. Little information could be gained from the maximum pressure array and this data are not considered here.

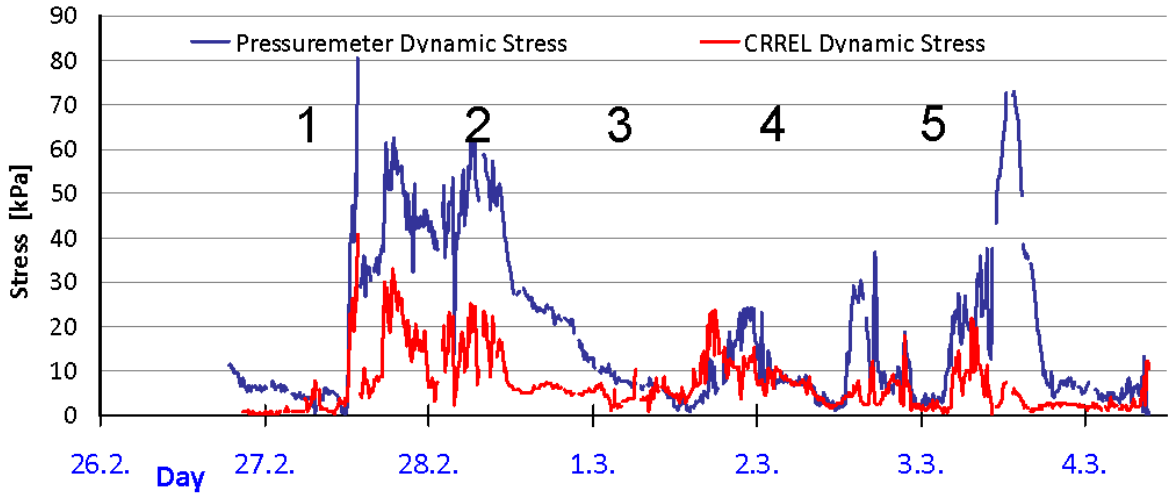

Figure 7. The dynamic stress estimates from the pressure cell array and from the biaxial stressmeter of the CRREL buoy. Days are numbered 1-5 for easier reference.

What strikes the most is the different overall level of the records. The pressure cell array values are typically two times higher than the biaxial stressmeter values. The mean values of the pressure cell and biaxial stressmeter records are 18.60 kPa and 6.9 kPa and the maxima 80.4 kPa and 40.6 kPa respectively. There is variation in this respect however. The stress signatures on days 1 and 2 are more or less scaled copies, by factor 2, of each other. The stress maxima occur at same times and the overall shapes are similar. On days 3 and 4, from noon to noon, the stress maxima are on the same level. For some reason the raising stress signal trails by four hours for the pressure cells but for the relieving stresses the records are

identical. On day 4 afternoon the 30 kPa pressure cell stresses are only weakly echoed by the biaxial stressmeter while in the evening the match is again almost exact. In a similar fashion on day 5 the correspondence by scale factor 2 is followed by 73 kPa peak for the pressure cell which has only a very weak although discernible counterpart for the biaxial stressmeter.

As the records are almost identical over several periods this indicates that there is no systematic error or difference in operating principle explaining the stress level differences. Ice thickness was also about the same for both. A possible explanation is different distance from floe edges of from 'hotspots' over which ice cover stresses are transmitted between floes.

Diverse deformation events added to the ridge and lead geometry close to the site during Phase 1 (Table 2, Figure 8). When the site was visited first time in the morning notes on the changes were made as well as later on those occurring at daytime. There were on day 1 two cracks A and B at distances 30 m and 200 m from the site. On day 2 crack A was found partially ridged; this event may relate to the stress peaks of preceding night. On day 3 there was opening and closing of leads but no deformation, and the stress levels remained low during daytime. The stress peaks in the evening of day 3 apparently relates to the closing and ridging of both A and B observed next morning. After a pause the deformations recommenced in the evening of day 4 and intensified during the night. This however shows only as 20-30 kPa peaks in the records while the 73 kPa record next day is from calmer conditions. It is apparently related to a new crack formed very close to the pressure cells.

There exist thus links between the observed deformations and stress record signatures. However, the highest peaks did no occur during the most intense observed ridging phase (around midnight between days 4 and 5) but rather when the deformation was moderate, during adjusting of the floe geometry. This was associated with some deformation at interfaces but still with intermittent contact between the floes. The proximity of the pressure cell array to the ridged section of crack A may also explain the higher stress level as this is a likely location for floe-floe stress transmittance.

Table 2. Discontinuities and deformation events at the stress site and surroundings. The biaxial stressmeter site remained integral during Phase 1.

Day 1 (27. Feb)	Crack A 2 m wide 30 m SE from the array edge Crack B 0.3 m wide 200 m W from the array edge
Day 2 (28. Feb)	Crack A partially ridged W from the array, otherwise 2 m wide Crack B unchanged
Day 3 (1. Mar)	Crack A open part widened, ridged part remains wide Crack B closed Leads opening between the site and R/V Aranda
Day 4 (2. Mar)	Crack A closed and ridged, sail 0.5-0.8 m high Crack B closed and in part ridged Crack C opened, runs in part parallell with A Crack D opened 150m NE from the array One crack trough the maximum array Leads between the site and R/V Aranda closing and ridging in the evening
Day 5 (3. Mar)	Crack A unchanged: ridged with 0.5-0.8 m high sail Crack B closed and ridged Cracks C and D unchanged Pressure cell not included to the rosette separated by a closed crack from others Maximum array pressure cells separated by a network of closed cracks New ridges formed around R/V Aranda during the night

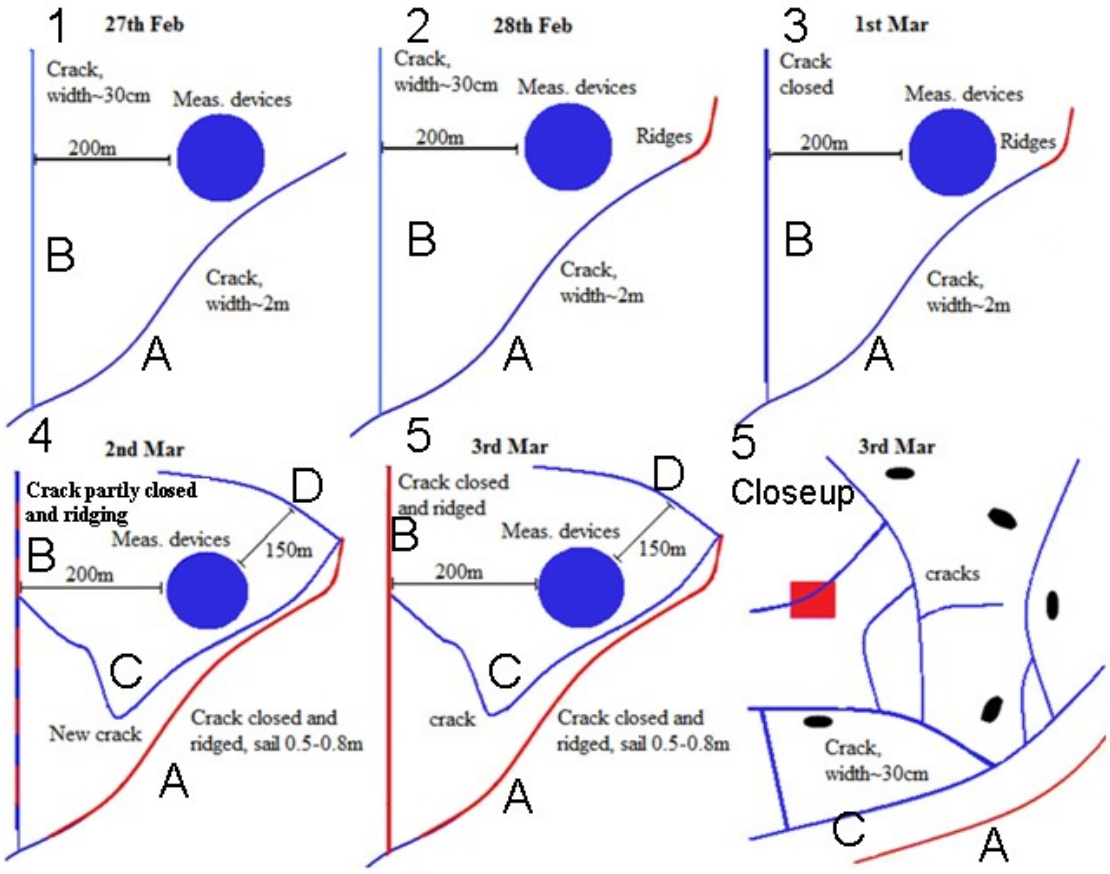

Figure 8. Cracks and ridge formation around the site. The blue circle covers the measurement site of Fig 6a. It is shown also in the close-up where red rectangle indicates the location of pressure cell array with logger and the black dots are maximum pressure array.

Phase 1 and 2: Relation to wind forcing and drift

The record from the biaxial stressmeter for Phases 1 and 2 is in Figure 9 that shows also wind speed and direction, and drift speed. During Phase 1 the events and records fit coherently together. There are periods of drift, driven by higher wind stress, and intervening inert periods. The wind direction appears to have its effect also. The formation of new cracks is associated with wind direction change (evenings of day 4 and 5) and two peaks occur at times of rapid direction change (day 3 noon, day 5 after midnight). The pressure cell array peak of day 5 (Figure 7) occurs also after wind direction change when the drift has ceased and the wind speeds are about half from those during the ridging period of the preceding night.

During Phase 2 the picture looks more complicated. A period of fast drift follows between 2nd and 3rd March but without stresses. This may relate to the lead and crack geometry the changes of which were not observed after Phase 1. The drift also ends with a stress peak at the time of highest wind speed. This suggests that maximum compactness is again attained but ridging is not set on.

After this follows a two-day period (4th and 5th March) during which the wind speeds decrease and wind direction turns to NW quadrant. There is a short drift period but otherwise the ice cover is inert. The stresses however are seen to gradually increase until the highest observed value 73 kPa is attained; this is the situation of Figure 5. As the winds turn back to SW quadrant the stresses are relieved and a period of constant wind speed and fast drift without stresses follows. One more stress peak follows, associated with decreasing drift speed.

The interpretation appears clear. The NW quadrant winds compacts the ice cover towards the Finnish coastline but wind speeds are too low to set on ridging. This gradually increases the stresses. As the wind turns back to SW quadrant the ice begins to drift along coast in almost free-drift manner unless the stresses build up again after 8th March. This corroborates the previous observations that highest stresses are not attained during ridging but when a somewhat shuffled arrangement of ice cover geometry seeks to adjust anew to maximum compactness.

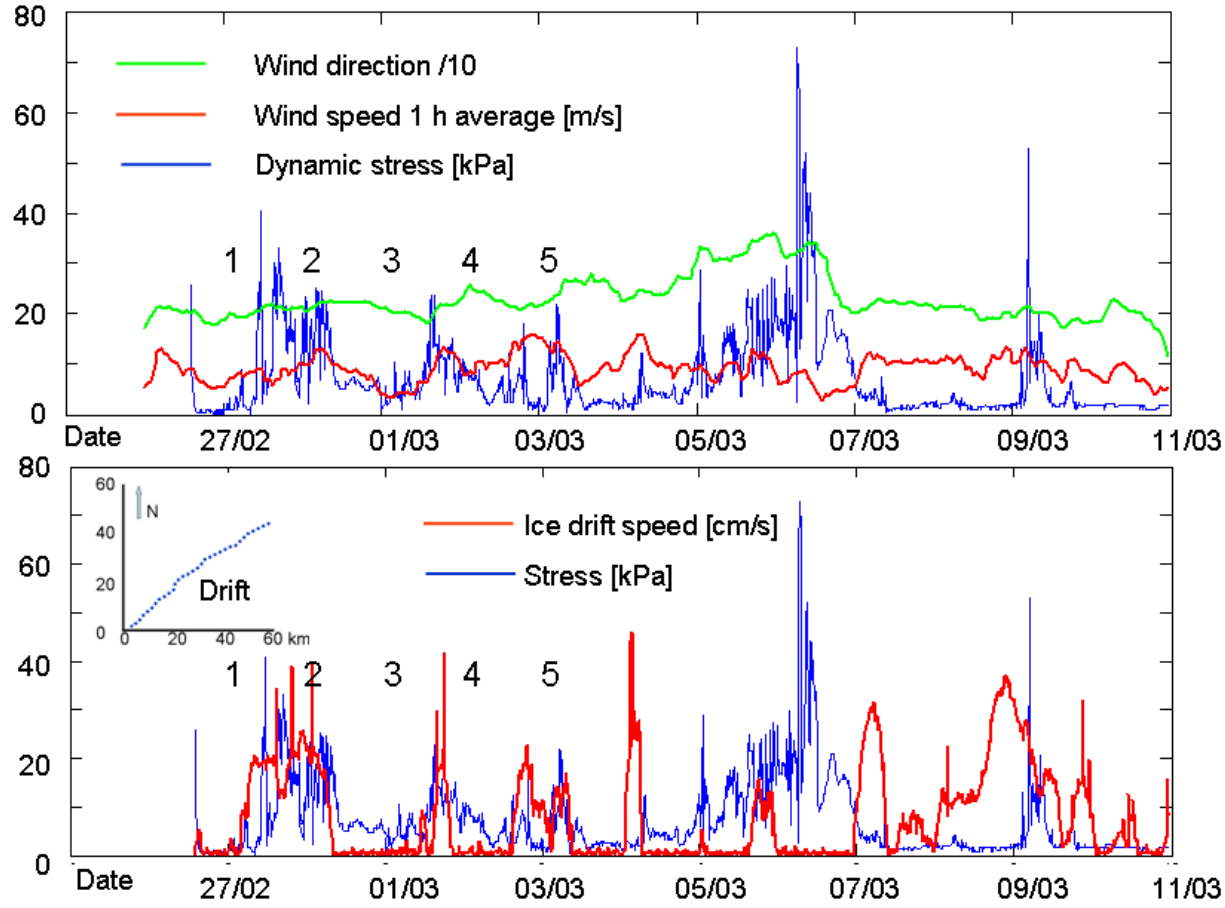

Figure 9. The biaxial stressmeter record with wind and ice drift data. Days 1-5 of Phase 1 marked as well.

DISCUSSION

The results from a two-week ice stress measurement campaign in the Baltic have been described. Although the records were short in comparison with previous Arctic campaigns, which have lasted months, a wealth of results could be extracted. Two instrument types were used: biaxial vibrating wire stressmeters, and simple pressure cells with attached pressuremeters. The dynamic stress estimates from both agreed generally well which demonstrates the applicability of relative cheap pressure cells to pack ice stress measurements. No conclusive explanation for the higher stress level of the pressure cells was found, and new campaigns with closer arranging of the two instruments are needed to answer this.

The maximum dynamic stress values were about 80 kPa. These are lower than the values found in the arctic, typically 200 kPa, but this can be explained by the shortness of the records

and a Baltic Sea campaign continuing throughout the whole ice season is expected show values similar to the Arctic observations (Lensu and others 2013b).

Several mechanisms behind the observed stress peaks could be identified. The basic distinction can be made between static and drifting ice cover and high values can be found in both. It appears however that the stresses do not simply increase with the intensity of drift and deformation. Highest stresses were observed from a static ice cover during moderate winds and there were indications that local contact geometry between floes has a decisive role. This corroborates the ice navigation community's observation that high compression is not associated with ongoing ridging but rather with an ice cover where ridging is just about to begin, and that there are certain geometry dependent 'hotspots' that are more prone to generate compressive situations. This agrees also with observations made in shorter length scales on local ice deformation, for example failing against a structure or ridge formation: the stresses are localised and the stress level is reduced after the onset of the deformation.

The physical phenomenon behind back ice stresses is the stress propagation in the complicated ice cover geometry composed of floes, leads, ridges and cracks. The temporal intermittency of the stress records can be assumed to be a counterpart of the spatial intermittency of the stress propagation (Lensu and others 2013b). This also agrees with other observations made by ice going ships: the compression is a localised phenomenon that can generate and disappear quite unexpectedly. However, reliable inferences from stress records to the spatial stress distribution and the probability of stress concentration occurrence would require more extensive campaigns involving several adjacent floes.

CONCLUSIONS

The results from a two-week ice stress measurement campaign in the Bay of Bothnia have been described. The stress records show similar characteristics as the Arctic records of previous campaigns but there are also basin specific features related to the nearness of coast. The stress peaks could be related with different contributing mechanisms including ice deformation events, ice drift phases, and wind direction and speed. The maximum stress values were about 80 kPa. Also the applicability of simple pressure cells in stress measurement arrays became demonstrated.

REFERENCES

Coon, M.D., Lau, P.A., Bailey, S.H., and Taylor, B.J., 1989. Observations of ice floe stress in the eastern Arctic. Proc. 10th POAC, Luleå, Sweden, vol. 1 pp. 44-53.

Cox, G.F.N and Johnson, J.B., 1983. Stress measurements in ice. US Army CRREL Rep. 83-23.

Croasdale, K.R, Comfort, G., Frederking, Graham, B.W., and Lewis, E.L., 1988. A pilot experiment to measure Arctic pack ice driving forces. In W.M. Sackinger and M.O. Jefferies (eds), Port and Ocean Engineering under Arctic Conditions, Univ. of Alaska, Vol III, pp. 381-395.

Lensu, M. , Elder, B., Richter-Menger, J. and Haapala, J., 2013b. Comparison of ice stress records in terms of extremal value analysis. Accepted for publication in Annals of Glaciology 54(62)

Lensu, M., Haapala, J., Lehtiranta, J., Eriksson, P., Kujala, P., Suominen, M., Mård, A., Vedenpää, L., Kõuts, T., Lilover, M., 2103a. Forecasting of compressive ice conditions. Proceedins of the 22nd International Conference on Port and Ocean Engineering under Arctic Conditions, POAC'13, June 9-13, Espoo, Finland (this volume).

Richter-Menge, J.A. and B.C. Elder 1998. Characteristics of pack ice stress in the Alaskan Beaufort Sea. J. Geophys. Res. 103, C10, pp. 21818-21829.

Richter-Menge, J.A., Elder, B., Claffey, K., Overland, J.E., and Salo, S., 2002. In situ sea ice stresses in the western arctic during the winter 2001-2002. Proc. 16th IAHR Int. Symp. on Ice, Dunedin, New Zealand, pp. 131-138.

Tucker, W. B. , III, and Perovich, D.K., 1992. Stress measurements in drifting pack ice. Cold Reg. Sci. Tech. 20, pp. 119-139.

Richter-Menge, J.A., McNutt, S.L., Overland, J.E.,and Kwok, R., 2002. Relating arctic pack ice stress and deformation under winter conditions. J. Geophys. Res. 107, C10, pp. SHE 15-1–SHE 15-13.